RSC Advances

This is an *Accepted Manuscript*, which has been through the Royal Society of Chemistry peer review process and has been accepted for publication.

Accepted Manuscripts are published online shortly after acceptance, before technical editing, formatting and proof reading. Using this free service, authors can make their results available to the community, in citable form, before we publish the edited article. This *Accepted Manuscript* will be replaced by the edited, formatted and paginated article as soon as this is available.

You can find more information about *Accepted Manuscripts* in the Information for Authors.

Please note that technical editing may introduce minor changes to the text and/or graphics, which may alter content. The journal's standard Terms & Conditions and the Ethical guidelines still apply. In no event shall the Royal Society of Chemistry be held responsible for any errors or omissions in this *Accepted Manuscript* or any consequences arising from the use of any information it contains.

ROYAL SOCIETY OF CHEMISTRY

www.rsc.org/advances

1 # *Ab initio* study on the stability of N-doped ZnO under high pressure

2 Xiaojing Sha, Fubo Tian, Da Li, Defang Duan, Binhua Chu, Yunxian Liu, Bingbing
3 Liu and Tian Cui*

4 *State Key Laboratory of Superhard Materials, College of Physics, Jilin University,*

5 *Changchun 130012, People's Republic of China.*

6 *Corresponding author, E-mail: cuitian@jlu.edu.cn, Tel. / Fax: +86-431-85168825*

7 We perform first-principles density functional theory calculations to examine the
8 stability of nitrogen-doped wurtzite ZnO under pressure. Our calculations indicate
9 that both the stability of the nitrogen-doped ZnO and the defect concentration
10 increase with pressure. As the pressure increases from 0 to 9 GPa, the density of
11 states at the Fermi level decreases, and the states have a tendency to move to lower
12 energy levels. Electron-localization function and Bader charge analysis have been
13 used to understand the pressure effect on the defect. Under the basic growth
14 conditions (using ε-N_2 for nitrogen atoms), the calculated formation enthalpies
15 decrease with pressure, which suggests a rise in the defect concentration. Applying
16 pressure has great impact on the nitrogen-doped defects, and can be used as an
17 efficient approach to form *p*-type ZnO.

18

RSC Advances Accepted Manuscript

1 Introduction

During the past years, wurtzite-ZnO has received great attention as a promising material for electronic, ferroelectric, and optical applications. ZnO has a direct band gap of 3.3 eV and a large exciton binding energy of 60 meV, thus it has drawn particular interests for potential applications in short wavelength optoelectronic devices, where the efficient excitonic UV laser actions have been demonstrated at room temperature.[1-3] N-type ZnO is available even without any intentional doping, and low-resistance n-type doping with electron concentrations as high as 10^{21} cm^{-3} has been achieved.[4] On the other hand, it is very difficult to obtain *p*-type ZnO[5], although recently it was demonstrated that high densities of holes could be obtained with N or As as the dopant using novel doping techniques.[6-9]

The properties of semiconductors are often controlled by defects and impurities, where the incorporation of impurities in small concentrations usually affects the electrical conductivity in a significant way. Nitrogen is thought to be the most suitable *p*-type dopant in ZnO mainly due to its similar atomic radius and electronegativity as O, and thus should readily substitute on O sites.[10] Although theory suggests some difficulties to achieve a shallow acceptor level in N-doped ZnO,[6,11,12] N is still considered as the most suitable dopant for its lower lattice distortion, compared with Al, Ga, and In doping.[13] Several mechanisms leading to the *p*-type difficulties are well known: low solubility, the compensation by low-energy native defects, deep impurity level, and structural stability known as AX and DX centers.[6,9,14] N-doped ZnO, the most feasible and promising candidate for *p*-type ZnO,[6,15-17] also suffers from the low doping efficiency and the instability of substitutional nitrogen.[18] Some nonequilibrium growth techniques have been used to greatly enhance the solubility of nitrogen dopants in ZnO, such as epitaxial and molecular doping (NO_2, NO, etc.).[19] Moreover, new advanced approaches to create more stable and shallower acceptors in ZnO are still a subject of intense research. First-principles calculations have become more and more powerful tools to help

RSC Advances Accepted Manuscript

1 explaining and supporting experiments, as well as predicting new materials and their
2 properties, especially at extreme conditions such as under high pressure. Some
3 first-principles total-energy calculations suggest shallow donor levels of the oxygen
4 vacancy V_O and zinc interstitial Zn_i, possibly responsible for the high n-type
5 conductivity and the equilibrium *p*-type doping difficulties in ZnO.[20] In previous
6 reports, Gai et al show that the formation enthalpies of these low energy intrinsic
7 defects decrease with pressure, indicating possible weaker effect of compensation and
8 favorable *p*-type doping at pressure.[21] So the pressure is an important means to
9 change the material properties.

10 Here we investigate the N-doped defects in ZnO under high pressure using a
11 first-principles pseudo potential method. To understand the pressure dependences, we
12 examine the geometry optimization, formation enthalpies and electronic structure of
13 the N-doped ZnO under pressure. We describe the methods used in the calculation in
14 Section 2, and present the calculated results and discussions of the defect formation
15 enthalpy, transition energy levels, pressure dependence of the bond length and
16 electronic structure in Section 3. The paper is concluded with a brief summary in
17 Section 4.

18 **2 Computational Details**

19 In this paper all structural optimizations, electronic band structure calculations
20 and defect formation enthalpies for ZnO were performed using the Vienna *ab initio*
21 simulation package (VASP)[22] utilizing the projector augmented plane-wave (PAW)
22 method[23,24] to describe the core-valence interaction. For structure optimization, the
23 exchange correlation (XC) functional was treated within the Ceperley-Alder LDA
24 (CA-LDA) [25]. All calculations were performed treating Zn 3d electrons as valence
25 electrons. The cut-off energy set to be 550 eV, and the appropriate Monkhorst-Pack
26 K-point mesh were used with the resolution of $2\pi\times0.03 Å^{-1}$ for Brillouin zone (BZ)
27 sampling to ensure that all the enthalpy calculations were well converged to less than
28 1 meV, and 72-atom cubic supercell in the wurtzite structure for all defect

RSC Advances Accepted Manuscript

1 calculations. In all calculations, the volumes are fully relaxed until the
2 Hellmann-Feynman forces acting on the atoms become less than 0.01eV $Å^{-1}$.
3 The LDA band-gap error is caused by the cation-d states in II-VI band. Surely,
4 calculations in the GW approximation which largely correct for the LDA band-gap
5 error for ZnO, that the occupied cation-d bands shift down relative to LDA. In
6 research of Lany and Zunger, they used LDA+U method[26] to yield agreement of the
7 d-like density of states, and found the transition energies of V_{anion} calculated from
8 LDA+U supercell eneries differ only slight. The formation and transition energies
9 presented in those work are obtained using supercell total energies that are calculation
10 in LDA.[27] In our paper, we also calculate with LDA, as many other researchers in the
11 same way.[28, 29]
12 We use first-principles supercell calculations in order to determine the enthalpy
13 (H) at different volumes as $H=E+PV+qE_F$, where E_F is the Fermi level and q is the
14 defect charge in electron units. $V = \partial H/\partial P$ defines the formation volume and
15 determines the pressure dependence of the formation enthalpy. Under hydrostatic
16 pressure, the change of crystal volume depends on both the internal strain introduced
17 by the defect and external pressure $\Delta V^f_D=\Delta V_T-\Delta V_P$. ΔV_T is the total volume change
18 of the supercell containing defect under hydrostatic pressures, ΔV_P is the volume
19 change caused by external pressure, and ΔV^f_D is the change of ideal crystal volume
20 caused by the defect under hydrostatic pressure. Therefore, ΔV^f_D should be a constant
21 for a given defect and is a symbol of defect concentration dependent on pressure.
22 The formation enthalpy of dopants has an influence on the solubility and thus
23 the carrier density. The defect equilibrium concentration c in the thermodynamic
24 equilibrium is related to the defect formation enthalpy H^f by:
25
$$c = N_{sites} \exp\left(-H^f/k_B T\right) \qquad (1)$$
26 N_{sites} is the number of sites per unit volume, where the defect is incorporated into, k_B
27 is the Boltzmann constant, and T is the temperature. The formation enthalpy of defect
28 nitrogen substituted for oxygen (N_O) in charged state q is defined as:[30]

RSC Advances Accepted Manuscript

1 $$H^f(N_O, q) = H(N_O, q) - H(ZnO) + \mu_O - \mu_N + qE_F \qquad (2)$$

2 Here, H (N_O, q) is the total enthalpy of the supercell with defect N_O in a charge state q,
3 H(ZnO) is the enthalpy of the pure supercell without any defect, μ_i is the chemical
4 potential of species i in reference to the elemental solid /gas states, q is the number of
5 electrons transferred from the supercell to the reservoirs to form the defect cells. E_F is
6 the Fermi level with respect to the valence-band maximum (VBM). Both the
7 formation enthalpy and consequently the concentration of neutral defects strongly
8 depend on the host-element chemical potentials μ_{Zn} and μ_O, which are determined by
9 the growth conditions. Under equilibrium conditions, the concentration of a point
10 defect is mainly related to its formation enthalpy, which depends on the chemical
11 potentials of the host elements (in this case, Zn and O) and relevant impurity element
12 (N) as defined by appropriate reservoirs.[31, 32]

13 As we know, if the system contains an excess of O, the excess O may form a
14 bulk O precipitate. Consequently, the chemical potential of bulk O may not exceed
15 the chemical potential of bulk O, $\mu_O \leqslant \mu_{(bulk\ O)}$. Similarly, the chemical potential of Zn
16 may not exceed that of bulk Zn, $\mu_{Zn} \leqslant \mu_{(bulk\ Zn)}$. In addition, the sum of the O and Zn
17 chemical potentials is required to equal the chemical potential (per pair) of bulk ZnO
18 (We use the total enthalpy of a perfect ZnO cell at T = 0 K for μ_{ZnO}), $\mu_{ZnO} = \mu_{Zn} + \mu_O$.
19 And we have neglected the temperature dependence of E_g and ΔH. In our calculations,
20 we take the effects of stress into account, so we simply take the N_2 (in ε-N_2) as the N
21 source[33], and take the oxygen O8 as the O source.[34]

22 The formation enthalpy for each charged state of defect is calculated from the
23 total enthalpy. For all the defects considered here, the defect and hole concentrations
24 are determined by the charge neutrality condition.[35] For the charged defects a
25 homogeneous compensating background charge was added. We adjust the charge
26 through the parameter NELECT in the code, which equals to the total number of
27 electrons in the system plus the number of charged impurities.

28 The thermodynamic transition level of a defect between two different charge
29 states q and q', ε(q/q'), corresponds to the Fermi level at which the formation

RSC Advances Accepted Manuscript

1 enthalpies for the two charge states equalize. In reference to the Valence-Band
2 Maximum (VBM), the thermodynamic transition level is given as

3 $$\varepsilon(q/q') = (\Delta H^{q}_{f,VBM} - \Delta H^{q'}_{f,VBM})/(q' - q) \qquad (3),$$

4 where $\Delta H^{q}_{f,VBM}$ denotes the defect formation enthalpy for charge state q with the
5 Fermi level located at the VBM ($\Delta\varepsilon_F = 0$). The position of the thermodynamic
6 transition level, measured from the VBM as given in equation, or measured from the
7 conduction band minimum (CBM), corresponds to the ionization energy of a defect,
8 i.e. an acceptor or donor energy. [14]

9 **3 Results and discussion**

10 Before discussing the doped ZnO, we consider the structural properties of pure
11 ZnO. ZnO mostly crystallizes in hexagonal wurtzite-type structures (B4) at ambient
12 pressure, and it can also be stable in the cubic zinc-blende structure (B3) by
13 experiment.[36] At about 9 GPa, ZnO transits to the rock-salt structure (B1). Hence our
14 mainly discussion is with the B4 phase under 9 GPa. However, we performed the
15 calculations with B1 and B3 phase as a reference also. The optimized lattice
16 parameters of pure ZnO in B4 phase are a =3.195 Å and c=5.167 Å, which are in an
17 agreement with the experimental data of 3.245 Å and 5.209 Å.[11]

18 Figure 1 shows the calculated defect formation enthalpy of the nitrogen doped in
19 ZnO (N_O), under both the O-rich and Zn-rich growth conditions, at 0, 5 and 9 GPa, as
20 a function of the Fermi energy. We examine ZnO in the B4 phase under pressures up
21 to 9 GPa, below which the B4 structure is known to be stable. The changes in the line
22 slopes represent different defect charged states, while the corresponding transition
23 levels are marked with vertical lines. The defect formation enthalpies depend strongly
24 on the Fermi level for the charged states. N_O has the lower formation enthalpies under
25 the Zn-rich condition, than under the O-rich condition. Janotti et al. previously
26 reported that oxygen vacancies have the lowest formation enthalpies and act as the
27 dominant defect species under Zn-rich condition.[37] Thus, less energy is generally
28 required for N atom to enter into the oxygen vacancy sites. As shown in Figure 1, in

RSC Advances Accepted Manuscript

N-doped ZnO where the Fermi level is high in the band gap, the negatively charged cation vacancy has lower formation enthalpy which decreases with pressure, but the pressure dependence is less significant than the neutral part. Under both Zn-rich and O-rich conditions, the defect formation enthalpies decrease with the pressure increasing. That indicates that with the pressure increasing, the structure is becoming more stable.

The defect formation volumes obtained via equation and the formation volumes of N_O under 0, 5, and 9 GPa are -0.64, -0.63, and -0.59 $\Omega_{f.u.}/e$ ($\Omega_{f.u.}$ denotes the volume per formula unit),[38] respectively. The defect formation volume of N_O is always negative under different pressures. Thus, according to $V = \partial H/\partial P$, the formation enthalpy would decrease with pressure in principle, which contrasts our calculations in formation enthalpy.

Based on the defect formation energies, the equilibrium defect concentrations were estimated by the equation (1). The defect concentrations of N_O at different temperatures and pressures can be read from Fig.2. We consider has the ZnO annealed at high temperature, typically 1300 K.[39] At high temperatures, the defects can diffuse sufficiently rapidly that their concentration reaches equilibrium. For example, if materials were synthesized at 1300 K, the No concentrations under 0, 5, 9 GPa would be 2.79×10^{16}, 1.13×10^{17}, and 1.39×10^{17} cm^{-3}, respectively. The calculated concentration in ZnO is in good agreement with the reported value of ~1×10^{17} cm^{-3}.[40] As fig. 2 shown, the equilibrium concentration of N_O will increase when the pressure increases.

The electron-localization function (ELF) of N_O was calculated under 0, 5 and 9 GPa. At 0 GPa, as shown in Figure 3, significant charge density contours can be seen between the Zn and the O atoms, as well as the Zn and N atoms, and the ionic bonding usually prevails for ZnO. After compared the ELFs between 0 and 9 GPa, we find there is very little differences between the bonds and the charge density, which can be also seen from the respective values of Bader charges at different pressures, as shown in Table I. At atomic state, the charges of Zn and N atoms are 12

RSC Advances Accepted Manuscript

1 and 5 respectively. With pressure increasing, N atoms accept more charges from Zn
2 atoms, with the charge number raised from 6.37, 6.38 to 6.39, indicating stronger
3 ionic bonds between Zn and N. For 0 to 9 GPa is a lower pressure range, the change
4 of charge is inconspicuous. The Bader charges has been calculated with the B3 phase,
5 in which phase the atoms have the same coordination number with B4 phase. From
6 10, 30, and 60 GPa, the charge number is 6.42, 6.45, and 6.50, respectively. From the
7 large pressure range, there is an obvious change of charge under pressure between Zn
8 and N. So, the bond between Zn and N is stronger, when the pressure is increasing.
9 We examine both the undoped and N-doped ZnO using supercell approach.
10 Figure 4 shows the calculated total density of states (DOS) for the bulk ZnO host
11 (dash line) and N-doped ZnO (full line) at ambient pressure, in which the zero energy
12 is set at the Fermi level. The Fermi energy, E_F, is defined as the highest energy value
13 of an occupied state in the system inside the first Brillouin zone[37]. The calculated
14 band gap of undoped ZnO is 0.9 eV. The values of the band gap calculated using the
15 GGA are generally underestimated, in comparison to the experimental data (3.2 eV,
16 Ref. 41). As shown in Figure 4, a defect band is generated at the top of the valence
17 band for *p*-type N-doped ZnO, comparing to the DOS of undoped ZnO. For the
18 *p*-type ZnO:N, we further examine the pressure dependence of the electronic
19 structure form the partial DOS (PDOS), as shown in Figure 5. The electronic
20 structure of the valence band at the Fermi level are mostly from 2p states of N atoms,
21 Zn 3p states and Zn 3d states. Those states are hybridized and the hybridization effect
22 becomes further profound with the increase in pressure. The PDOS are calculated
23 under different pressures (P= 0, 5 and 9 GPa). The corresponding values of DOS at
24 the Fermi level are about 33.33, 28.78 and 27.35 states/eV/cell, respectively. The
25 decrease in the DOS value at the Fermi surface and the shift of the impurities peaks
26 to the lower energy both make the system more stable under pressure.[42] The
27 decreased defect formation enthalpies at pressure is previously shown to be related to
28 the stronger bond energy from the structure property, which can be further understood
29 from the electronic structure perspective here: the system become more stable as the

RSC Advances Accepted Manuscript

hybridization effect becomes further profound with the increase in pressure, and the value of DOS at Fermi level decrease.

The calculated formation enthalpies for N_O in ZnO are shown in Figure 1. N_O is stable in both the neutral and -1 charge states, with the acceptor level (0/-1) at 0.2 eV, consistent with previous results.[43] The calculated acceptor level (0/-1) using hybrid functional (1.3 eV) by Lyons et al., is significantly larger than our GGA results, which might be attributed to a noticeable downward shift of the VBM on an absolute energy scale. The transition levels remain unchanged under pressure, in both Zn-rich and O-rich situations, as shown Figure 1, indicating that pressure has little influence on the transition levels.

From the previous study,[44] the formation enthalpies of V_O, Zn_O, and Zn_i increased with pressure increased, and the formation enthalpies of V_{Zn}, O_{Zn}, and O_i decreased with pressure increased. In the investigation of cation vacancies in GaN, AlN, and GaAs[45], they found the formation enthalpies of cation vacancies in AlN, GaN, and GaAs decreased with pressure increased. To analysis the effect of different ions substitution, we also discuss the situation of Na substituted for Zn. In our calculation, the formation enthalpy of Na_{Zn} increased with pressure, which is opposite with the results of N_O. The phenomenon shows the cation substitutional defect becomes unstable with pressure is same with the native defect of V_O, Zn_O, and Zn_i, indicated that the change of formation enthalpy under pressure is influenced by the defect type.

4 Summary

We have studied the stability of N-doped ZnO under pressure via first-principles DFT calculations. Introducing high pressure results in a decrease in the formation enthalpy, and an increase in the equilibrium concentration of N_O. The calculated values of defect formation volumes are always negative, indicated the formation enthalpy would decrease with pressure. With the increasing pressure, the impurities energy level located at Fermi energy are weakened. The Bader charge analysis shows

RSC Advances Accepted Manuscript

1 that pressure also makes bond energy stronger. Overall, pressure provides an efficient
2 way to approach *p*-type ZnO.

3 **Acknowledgement**

4 This work was supported by the National Basic Research Program of China (No.
5 2011CB808200), Program for Changjiang Scholars and Innovative Research Team in
6 University (No. IRT1132), National Natural Science Foundation of China (Nos.
7 51032001, 11074090, 11104102, 10979001, 51025206, 11204100), and National
8 Fund for Fostering Talents of basic Science (No. J1103202). Parts of the calculations
9 were performed at the High Performance Computing Center (HPCC) of Jilin
10 University.

RSC Advances Accepted Manuscript

1

2 **References**

3 1. D. Bagnall, Y. Chen, Z. Zhu, T. Yao, S. Koyama, M. Y. Shen and T. Goto, *Appl.*
4 *Phys. Lett*., 1997, **70**, 2230-2232.
5 2. Z. K. Tang, G. K. L. Wong, P. Yu, M. Kawasaki, A. Ohtomo, H. Koinuma and Y.
6 Segawa, *Appl. Phys. Lett*., 1998, **72**, 3270-3272.
7 3. U. Ozgur, Y. I. Alivov, C. Liu, A. Teke, M. A. Reshchikov, S. Dogan, V. Avrutin,
8 S. J. Cho and H. Morkoc, *J. Appl. Phys*., 2005, **98**, 103.
9 4. T. Minami, H. Sato, H. Nanto and S. Takata, *Jpn. J. Appl. Phys*., 1985, **24**, L781.
10 5. S. B. Zhang, S.-H. Wei and A. Zunger, *J. Appl. Phys*., 1988, **83**, 3192-3196.
11 6. C. Park, S. Zhang and S.-H. Wei, *Phys. Rev. B*, 2002, **66**, 073202.
12 7. M. Joseph, H. Tabata and T. Kawai, *Jpn. J. Appl. Phys*., 1999, **38**, L1205.
13 8. Y. R. Ryu, S. Zhu, D. C. Look, J. M. Wrobel, H. M. Jeong and H. W. White, *J.*
14 *Cryst. Growth*, 2000, **216**, 330-334.
15 9. Y. F. Yan, S. B. Zhang and S. T. Pantelides, *Phys. Rev. Lett*., 2001, **86**, 5723.
16 10. D. W. Jenkins and J. D. Dow, *Phys. Rev. B*, 1989, **39**, 3317.
17 11. J. L. Lyons, A. Janotti and C. G. Van de Walle, *Appl. Phys. Lett*., 2009, **95**,
18 252105-252103.
19 12. Q. Wang, Q. Sun and P. Jena, *New J. Phys*., 2009, **11**, 14.
20 13. A. Mohanta, J. G. Simmons, H. O. Everitt, G. Shen, S. M. Kim and P. Kung, *J.*
21 *Lumines*., 2014, **146**, 470-474.
22 14. S.B. Zhang, *J. Phys.:Condens. Mat*., 2002, **14**, R881.
23 15. A. Tsukazaki, A. Ohtomo, T. Onuma, M. Ohtani, T. Makino, M. Sumiya, K.
24 Ohtani, S. F. Chichibu, S. Fuke and Y. Segawa, *Nat. Mater*., 2004, **4**, 42-46.
25 16. Y. Nakano, T. Morikawa, T. Ohwaki and Y. Taga, *Appl. Phys. Lett*., 2006, **88**, 3.
26 17. L. Shen, R. Q. Wu, H. Pan, G. W. Peng, M. Yang, Z. D. Sha and Y. P. Feng, *Phys.*
27 *Rev. B*, 2008, **78**, 4.
28 18. L. Wang and A. Zunger, *Phys. Rev. Lett*., 2003, **90**, 256401.
29 19. H. Matsui, H. Saeki, T. Kawai, H. Tabata and B. Mizobuchi, *J. Appl. Phys*., 2004,

RSC Advances Accepted Manuscript

1 **95**, 5882-5888.
2 20. L. Liu, J. Xu, D. Wang, M. Jiang, S. Wang, B. Li, Z. Zhang, D. Zhao, C.-X.
3 Shan and B. Yao, *Phys. Rev. Lett.*, 2012, **108**, 215501.
4 21. Y. Gai, B. Yao, Y. Li, Y. Lu, D. Shen, J. Zhang, D. Zhao, X. Fan and T. Cui, *Phys.*
5 *Lett.* A, 2008, **372**, 5077-5082.
6 22. G. Kresse and J. Furthmuller, *Phys. Rev. B*, 1996, **54**, 11169.
7 23. P. E. Blochl, *Phys. Rev. B*, 1994, **50**, 17953.
8 24. G. Kresse and D. Joubert, *Phys. Rev. B*, 1999, **59**, 1758.
9 25. D. M. Ceperley and B. J. Alder, *Phys. Rev. Lett.*, 1980, **45**, 566.
10 26. A. I. Liechtenstein, V. I. Anisimov, and J. Zaanen, *Phys. Rev. B*, 1995, **52**,
11 R5467(R).
12 27. Stephan Lany and Alex Zunger, *Phys. Rev. B*, 2005, **72**, 035215.
13 28. R. Vidya, P. Ravindran, H. Fjellvåg, B. G. Svensson, E. Monakhov, M.
14 Ganchenkova, and R. M. Nieminen, *Phys. Rev. B*, 2011, **83**, 045206.
15 29. F. Oba, S. R. Nishitani, S. Isotani, H. Adachi and I. Tanaka, *J. Appl. Phys.*, 2001,
16 **90**, 824.
17 30. S. Zhang and J. E. Northrup, *Phys. Rev.Lett.*, 1991, **67**, 2339.
18 31. D. B. Laks, C. G. Van de Walle, G. F. Neumark, and S. T. Pantelides, *Phys. Rev.*
19 *Lett.*, 1991, **66**, 648.
20 32. S. B. Zhang and J. E. Northup, *Phys. Rev. Lett.*, 1991, **67**, 2339.
21 33. X. Wang, Y. Wang, M. Miao, X. Zhong, J. Lv, T. Cui, J. Li, L. Chen, C. J.
22 Pickard and Y. Ma, *Phys. Rev.Lett.*, 2012, **109**, 175502.
23 34. L. Zhu, Z. W. Wang, Y. C. Wang, G. T. Zou, H. Mao, and Y. M. Ma, *Proc. Natl. Acad.*
24 *Sci. U.S.A.*, 2012, **109**, 751.
25 35. J. E. Northrup and S. Zhang, *Phys. Rev. B*, 1993, **47**, 6791.
26 36. C. Klingshirn, *Phys. Status Solidi B*, 2007, **244**, 3027.
27 37. R. Dovesi, B. Civalleri, R. Orlando, C. Roetti and V. R. Saunders, in *Reviews in*
28 *Computational Chemistry*, *Vol 21*, edited by K. B. Lipkowitz, R. Larter and T. R.
29 Cundari (Wiley-Vch, Inc, New York, 2005), Vol. 21, pp. 1-125.

RSC Advances Accepted Manuscript

1 38. P. Erhart, K. Albe, and A. Klein, *Phys. Rev. B*, 2006, **73**, 205203.
2 39. G. D. Mahan, *J. Appl. Phys.*, 1983, **54**, 3825.
3 40. D. C. Look, D. C. Reynolds, C. W. Litton, R. L. Jones, D. B. Eason, and G.
4 Cantwell, *Appl. Phys. Lett.*, 2002, **81**, 1830.
5 41. S. Pearton, D. Norton, K. Ip, Y. Heo and T. Steiner, *J. Vac. Sci. Technol. B*, 2004,
6 **22**, 932-948.
7 42. P. Zhang, B. T. Wang, C. H. He, and P. Zhang , *Com. Mater. Sci.*, 2011, **50**, 12.
8 43. E.-C. Lee, Y. S. Kim, Y. G. Jin and K. J. Chang, *Phys. Rev. B*, 2001, **64**, 085120.
9 44. X. Sha, F. Tian, D. Li, D. Duan, B. Chu, Y. Liu, B. Liu, and T. Cui, *Solid State*
10 *Commun.*, 2015, **201**, 130.
11 45. N. E. Christensen and A. Svane, *Phys. Rev. B*, 2002, **66**, 075210.
12

RSC Advances Accepted Manuscript

1

2 ## Captions

3 **Table I** Bader Charge of the N atom and the four nearest-neighbor Zn atoms under
4 different pressures. The plant of Zn1, Zn2 and Zn3 is parallel to the (001).
5 The line above the Zn4 and N is parallel to the Z-axis.

6 **Figure 1** The defect formation enthalpies of N-doped ZnO, at both Zn-rich (left) and
7 O-rich (right) conditions, as a function of the Fermi level.

8 **Figure 2** The concentration of defects as a function of synthesis temperature at
9 pressure of 0, 5, and 9 GPa.

10 **Figure 3** Electron localization function contour map for ZnO:N.

11 **Figure 4** Total DOS and partial DOS (PDOS) of N-doped ZnO. The Fermi energy is
12 set to zero.

13 **Figure 5** Partial DOS of 3d and 2p states of zinc, 2p state of nitrogen under 0 GPa (a)
14 and 9 GPa (b).

15

RSC Advances Accepted Manuscript

1

2 Table I

	0 GPa	5 GPa	9 GPa
N	1.37	1.38	1.39
Zn1	-1.26	-1.27	-1.27
Zn2	-1.26	-1.27	-1.27
Zn3	-1.26	-1.27	-1.28
Zn4	-1.20	-1.21	-1.22

3

RSC Advances Accepted Manuscript

1

2 Fig. 1

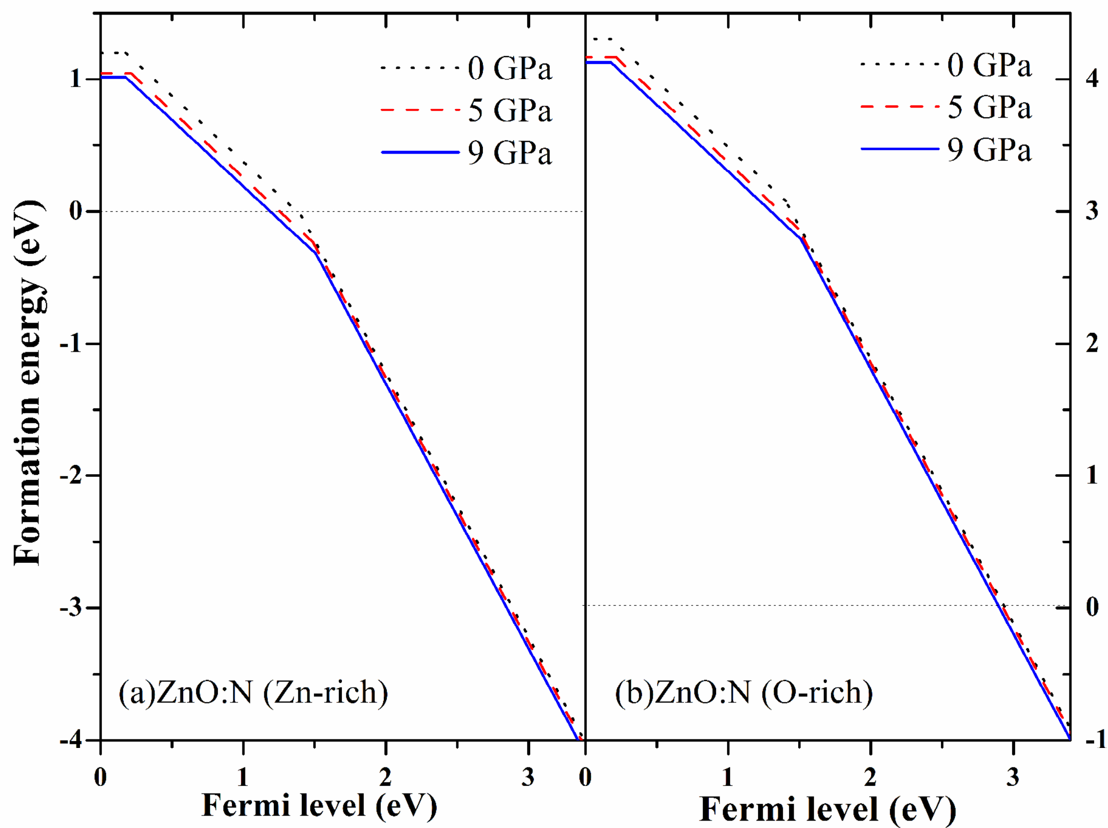

3

4

RSC Advances Accepted Manuscript

1 Fig. 2

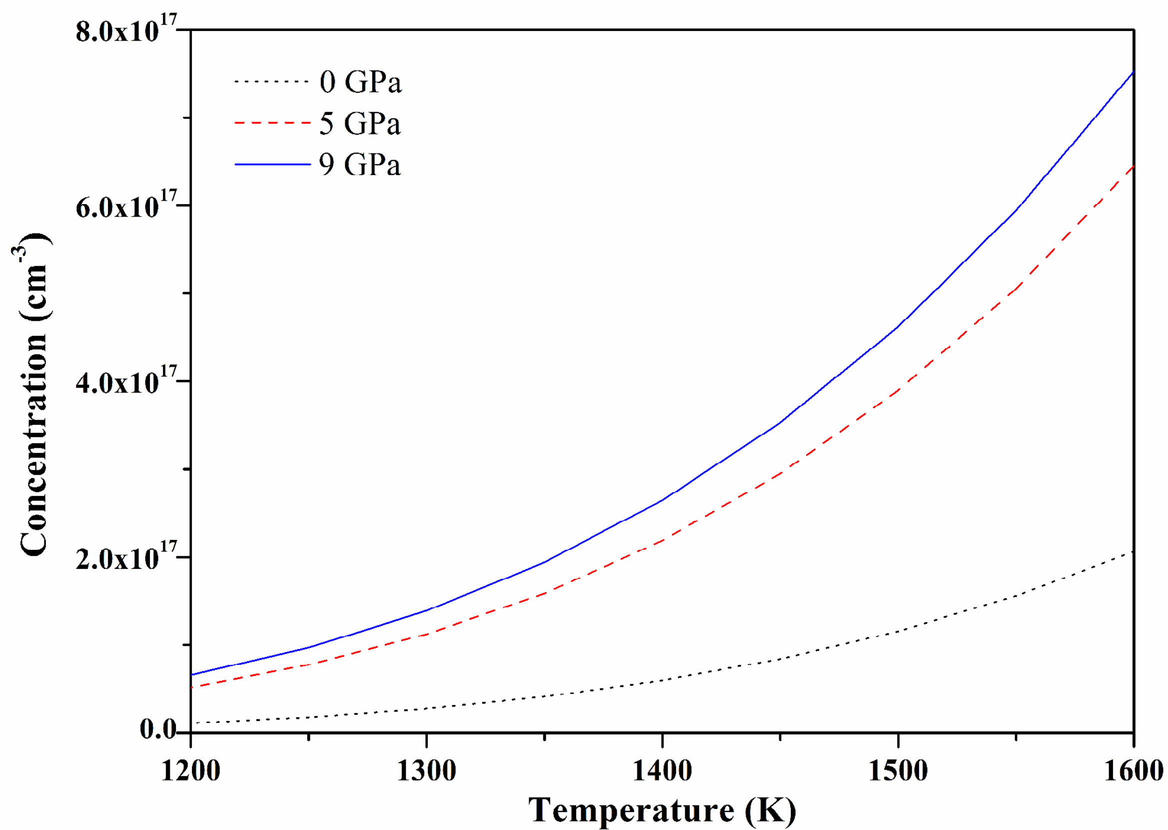

2

3

RSC Advances Accepted Manuscript

1 Fig. 3

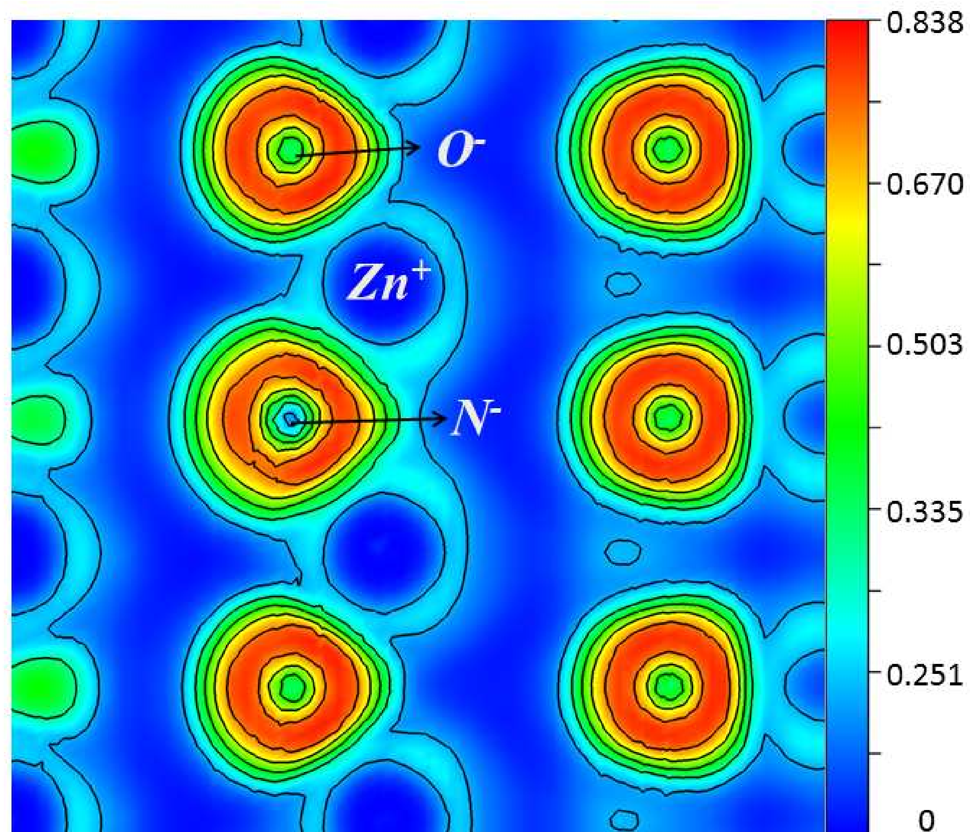

2

3

RSC Advances Accepted Manuscript

1 Fig. 4

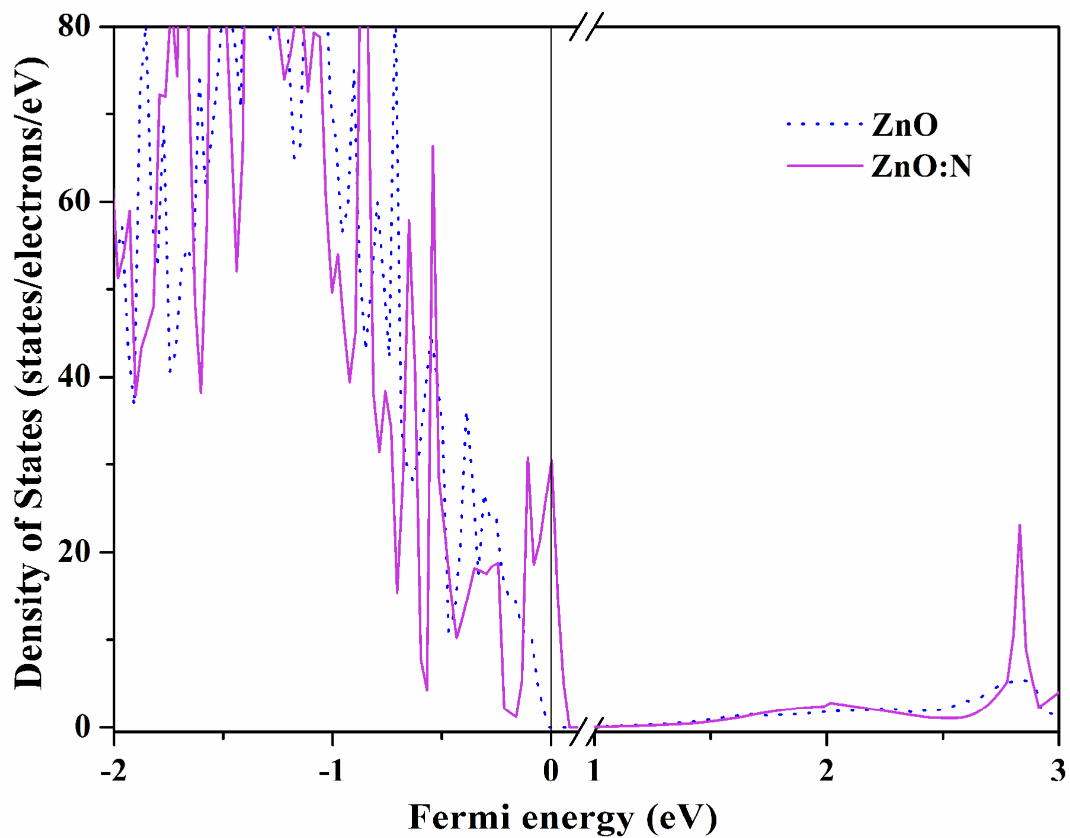

2

3

RSC Advances Accepted Manuscript

1 Fig. 5

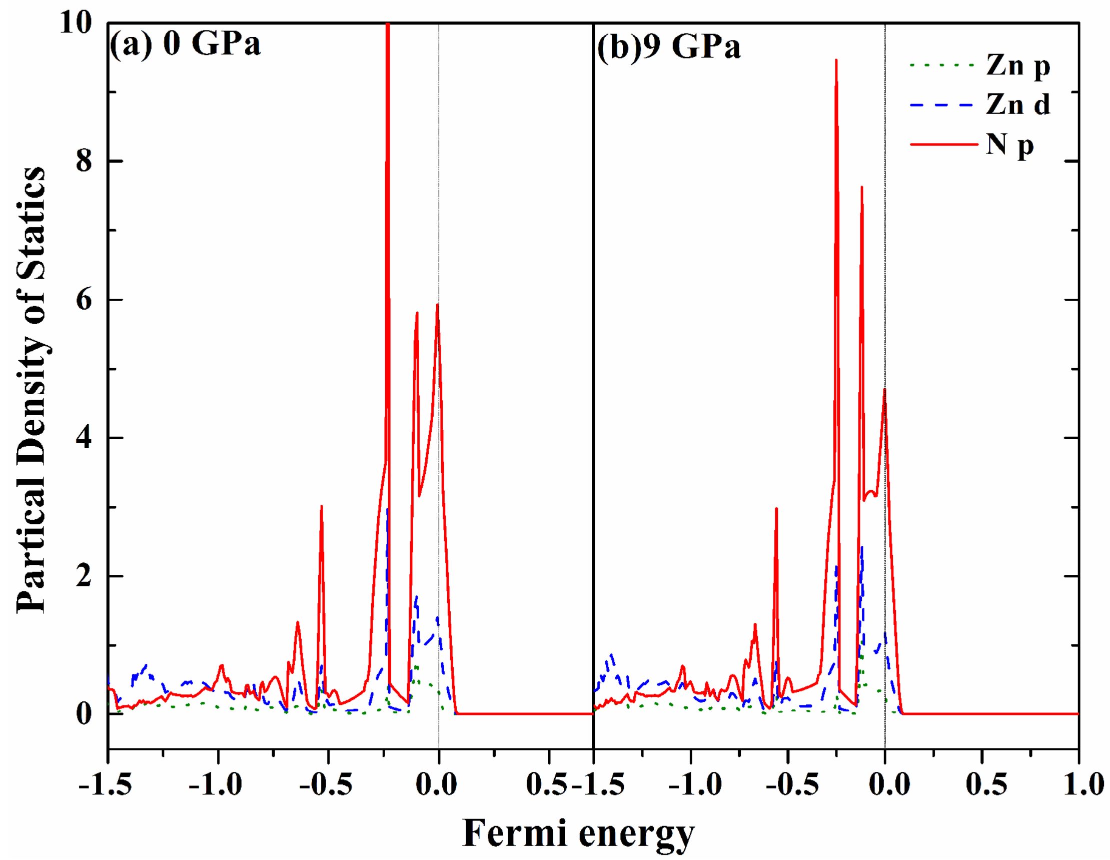

2

RSC Advances Accepted Manuscript

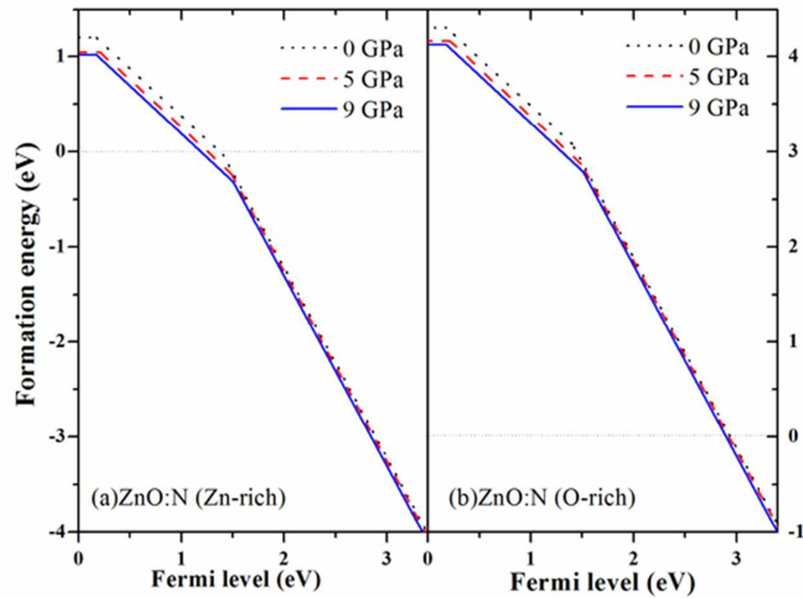

The defect formation enthalpies of N-doped ZnO, at both Zn-rich (left) and O-rich (right) conditions, as a function of the Fermi level.
57x40mm (300 x 300 DPI)

RSC Advances Accepted Manuscript

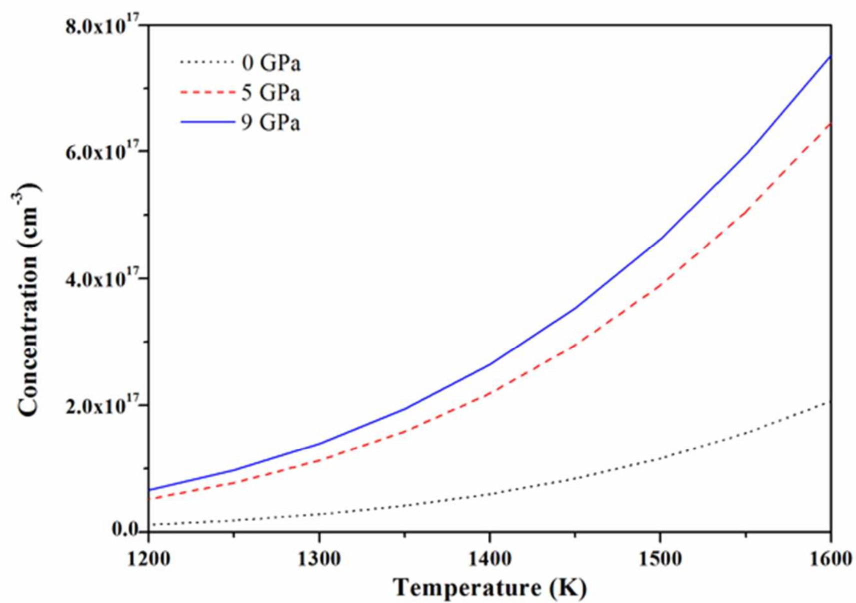

The concentration of defects as a function of synthesis temperature at pressure of 0, 5, and 9 GPa.
58x41mm (300 x 300 DPI)

RSC Advances Accepted Manuscript

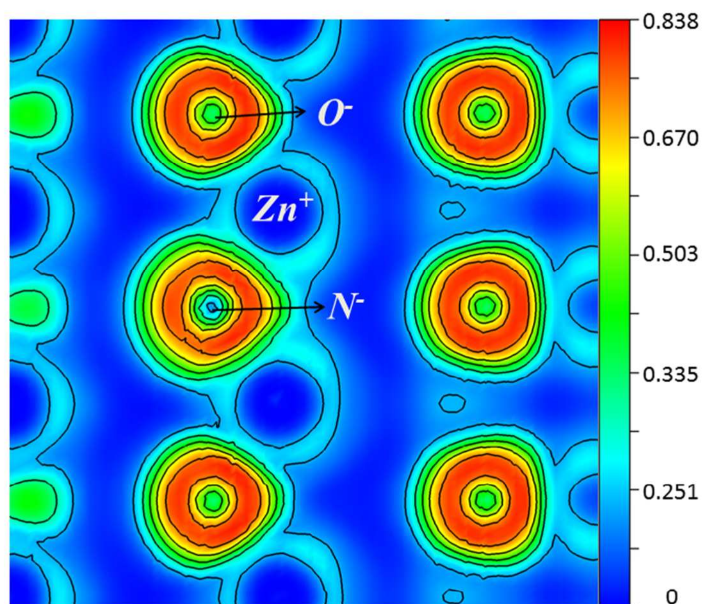

Electron localization function contour map for ZnO:N.
254x190mm (96 x 96 DPI)

RSC Advances Accepted Manuscript

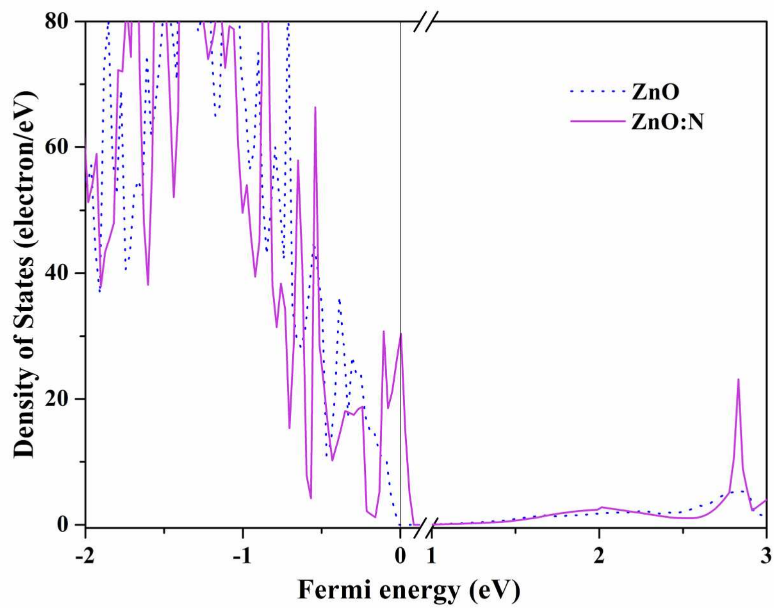

Total DOS and partial DOS (PDOS) of N-doped ZnO. The Fermi energy is set to zero.
210x148mm (300 x 300 DPI)

RSC Advances Accepted Manuscript

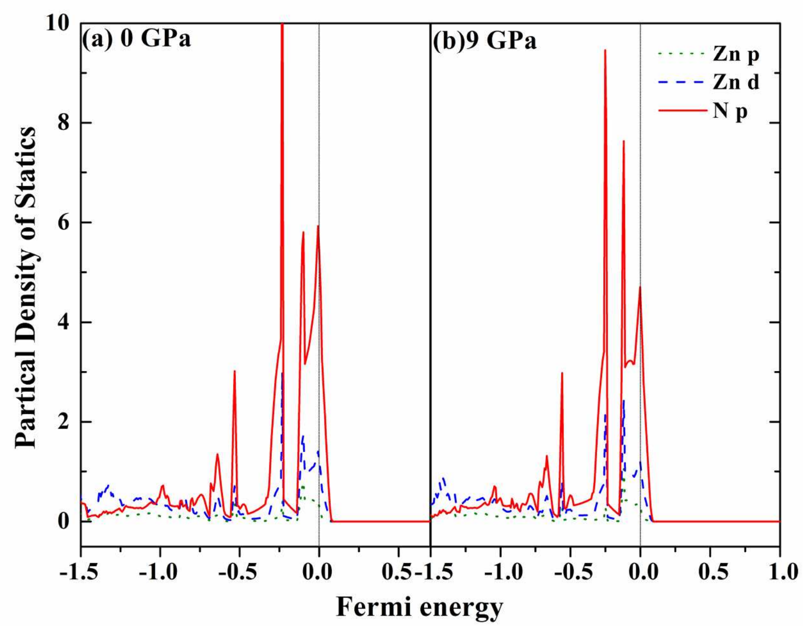

Partial DOS of 3d and 2p states of zinc, 2p state of nitrogen under 0 GPa (a) and 9 GPa (b).
202x141mm (300 x 300 DPI)

RSC Advances Accepted Manuscript